LBL-28256
Preprint

Lawrence Berkeley Laboratory
UNIVERSITY OF CALIFORNIA

Submitted to Journal of Statistical Physics

On the Universality Class Dependence of Period Doubling Indices

M. Feingold, D.L. Gonzalez, M. Magnasco, and O. Piro

December 1989

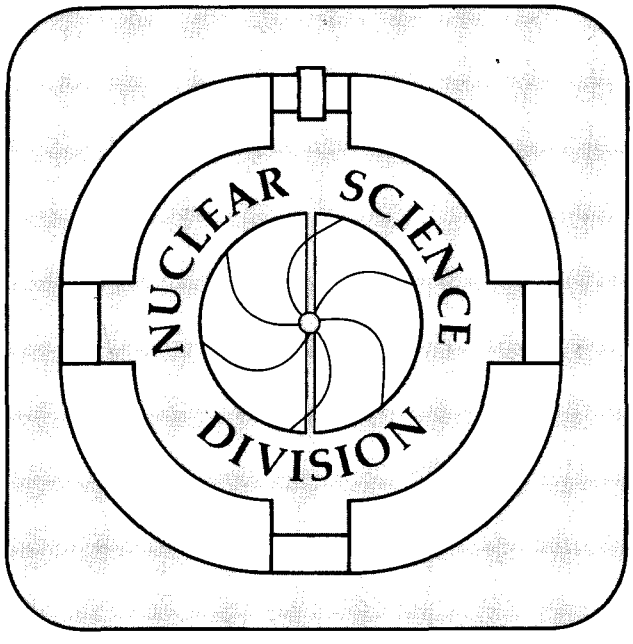

Prepared for the U.S. Department of Energy under Contract Number DE-AC03-76SF00098.

DISCLAIMER

On the universality class dependence of period doubling indices[†]

Mario Feingold,[1,4] Diego L. Gonzalez,[2] Marcelo O. Magnasco[1,2] and Oreste Piro[1,2,3]

[1] *The James Franck Institute, The University of Chicago, Chicago, IL 60637.*

[2] *Departamento de Física, Universidad Nacional de La Plata, C.C. 67, (1900)La Plata, República Argentina.*

[3] *Center for Nonlinear Studies, MB-S 258, Los Alamos National Laboratory, Los Alamos, NM 87544.*

[4] *Department of Physics and Lawrence Berkeley Laboratory, MS 70A-3307, University of California, Berkeley, CA 94720*

The dependence on ν of the period doubling scaling indices for unimodal maps with a critical point of the form $|x|^{\nu}$ is numerically investigated. To perform extensive computations of these indices a new symbolic dynamics based technique in configuration space is introduced. For $\nu \to 1$ it is shown that the Feigenbaum bifurcation rate converges to the theoretically exact value $\delta = 2$ limit only if $\nu - 1$ is exponentially small. On the other hand, the existence of an upper bound for $\delta(\nu \to \infty)$ is numerically verified. An accurate estimate of 29.8 is given for this limit. Moreover, the global functional form of $\delta(\nu)$ is shown to have an interesting symmetry.

PACS 05.45+b

[†] This work has been supported in part by the Director, Office of Energy Research, Office of High Energy and Nuclear Physics, Division of Nuclear Physics, of the U.S. Department of Energy under Contract No. DE-AC03-76SF00098.

1. Introduction

Period doubling universality is a well established theory.[1,2] It is well known, for instance, that the scaling behavior near the onset of chaos for unimodal maps of the interval[3,4] with a critical point of order $|x|^{\nu}$ only depends on ν.[5] In fact, ν labels the universality classes of unimodal maps which share the same scaling behavior. In other words, the indices describing such scaling are class functionals. Since the classes are only parametrized by ν, these indices are universal functions of ν. In particular, the bifurcation points in parameter space geometrically accumulate to the onset of chaos value with a rate δ and the highly bifurcated orbits scale around the critical point with a factor α. Both δ and α are universal functions of ν.[6] In the range $\nu \in (1, \infty)$, there are two singular limits in the scaling behavior. First of all, for $\nu \to 1$ the scaling factor α can be shown to diverge, and the bifurcation tree to collapse. This limit can be analyzed rigorously in the framework of renormalization group theory as a perturbation to the tent map. Such analysis leads to the result that $\delta(\nu \to 1) = 2$. Although the validity of the result is out of question, an accurate numerical check in the configuration space of the cascade is very difficult to achieve due mainly to the already mentioned divergence of $\alpha(\nu)$. At the opposite extreme, the other singular limit $\nu \to \infty$ is equally difficult to study numerically but at the same time is more controversial from the theoretical point of view. On one hand, first order renormalization schemes seem to predict a square root divergence of $\delta(\nu)$ as ν increases. This behavior is also suggested by earlier numerical results[7] for unimodal maps with high (≈ 40) ν. On the other hand, other renormalization group arguments[8,9,10] assure an upper bound of about 30 for $\delta(\nu)$.

The aim of this paper is to elucidate numerically the $\nu \to \infty$ limit for $\delta(\nu)$, not in a renormalization group framework, but rather by using its real space definition as the asymptotic rate of convergence for superstable parameter values. For this purpose, we introduce a map of infinite order in the sense that all its derivatives vanish at the critical point. In order to investigate the period doubling cascades in this extremely difficult

case, we developed a powerful numerical technique which we shall describe below. This tool is also appropriate to analyze with greater accuracy the limit $\nu \to 1^+$, which in turn is a good test for the reliability of the method. Finally, we speculate about the global form of the function $\delta(\nu)$ which shows a nice symmetry. Section 2 is devoted to the formulation of the problem and the introduction of the maps to be studied in the remainder. In Section 3 we devise the numerical method, discussing also its conceptual background. Section 4 contains the main results of our numerical work. We conclude in Section 5 with a discussion of these results and their implications.

2. The problem

Renormalization group arguments show that δ, the asymptotic ratio between the stability width of successive periods in a period doubling cascade, is only dependent on the order of the maximum for unimodal maps. Given a unimodal recurrence of the interval

$$x_{n+1} = f_\lambda(x_n) \tag{1}$$

which presents a period doubling route to chaos as λ is varied, this ratio is defined as

$$\delta_n = \frac{\lambda_n - \lambda_{n-1}}{\lambda_{n+1} - \lambda_n}, \quad \delta = \lim_{n \to \infty} \delta_n \tag{2}$$

where λ_n are the superstable points satisfying

$$f_{\lambda_n}^{2^n}(x_{\max}) = x_{\max} \tag{3}$$

for the 2^n cascade. λ_∞ is a critical point which lies on the border between the period doubling (or laminar) regime and the chaotic regime.

The second scaling index α (which is universal in the same sense as δ) is defined as

$$\alpha_n = \frac{d_n}{d_{n+1}}, \quad \alpha = \lim_{n \to \infty} \alpha_n \tag{4}$$

where

$$d_n = f_{\lambda}^{2^n - 1}(x_{\max}) - x_{\max} = \tag{5}$$

$$= \min_k \left(\left| f_{\lambda_n}^{k}(x_{\max}) - x_{\max} \right|, \quad k = 1 \cdots 2^n - 1 \right)$$

This index describes the way successive branches of the attractor scale around the maximum of f_{λ}, $x_{\max}$.

The Feigenbaum-Cvitanovic equation,

$$g(x) = -\alpha g \circ g\left(-\frac{x}{\alpha}\right) \tag{6}$$

fixes α and g for a given order of the maximum. Up to first order in a power series expansion, the following implicit equation for α can be obtained by direct substitution into Eq. (6)

$$\frac{\alpha^{\nu}}{\nu} - \alpha = 1 \tag{7}$$

where ν is the order of the maximum. A plot of $\alpha(\nu)$ vs. ν obtained from Eq. (7) is shown in Fig. 1. While this approximation for $\alpha(\nu)$ can differ from the exact values by as much as 15%, it gives essentially the correct asymptotic behavior.

Clearly, there are two singular limits:

a) $\nu \to 1$. In this limit the scaling factor $\alpha(\nu)$ diverges and accordingly the widths of successive branches decrease faster than exponentially. This behavior is suggested by the fact that the limit map is approximated in the neighborhood of the critical point by the so called *tent map*:

$$x_{n+1} = \lambda(1 - |2x_n - 1|) \tag{8}$$

For this particular case, all λ_n collapse to a single value $\lambda_0 = 1/2$ (*i.e.* the 2^n cycles appear all at once)[11] and the onset of chaos attractor shrinks to a single point in phase space. Nevertheless, renormalization group theory assures that $\delta(\nu \to 1) \to 2$.[4] Unfortunately, numerical checks of this prediction are extremely difficult and the best result

in the literature we are aware of[12] is $\delta(1.1) = 2.81$. Notice that the main obstacle in the way of these computations is the increasingly high value of $\alpha(\nu)$ as the limit is approached. Large α implies that branches born at a given bifurcation are separated by a distance which is tiny relative to that of their parents. Therefore, the resolution required to detect a bifurcation rapidly exceeds the available computational precision.

b) $\nu \rightarrow \infty$. Eq. (7) also shows that the scaling factor $\alpha(\nu)$ approaches unity in this limit. Consequently, the distance between branches in the neighborhood of the maximum does not scale geometrically from one generation to the next. On the other hand, there has been some controversy concerning the analysis of the asymptotic behavior of $\delta(\nu)$ in the renormalization group framework. While the power series truncation of the RG equations[7] seems to indicate that $\delta(\nu)$ diverges as $\sqrt{\nu}$, more general arguments[8,9,10] lead to an upper bound for $\delta(\infty)$. Assuming that an upper bound exists, neither an exact theoretical prediction nor an accurate numerical determination of its value is available at present.

An extremely important issue is the singularity of the double limit which leads to $\delta(\infty)$. The sequence of maps $f_\nu = 1 - k\,|\,x\,|^\nu$ approaches a discontinuous limit f_∞, which takes on the value of $-\infty$ for x outside of $[-1,1]$ and 1 inside. As a consequence, the chaotic region progressively shrinks in parameter space. Since the limit f_∞ has no dynamics, it is clearly impossible to calculate the scaling exponents while taking the $\nu \rightarrow \infty$ limit for the f_ν-family. It has thus been conjectured [10] that the correct way to take the limits is $\lim_{\nu \rightarrow \infty} \lim_{n \rightarrow \infty} \delta_n(\nu)$, and that the reverse order is meaningless. However, the above argument is based on the false assumption that all families of maps of this kind share the property of becoming discontinuous and flat in the limit. The value of δ is influenced solely by the shape of the function near the maximum, and a maximum of order ν certainly does not imply that the function should be homogeneous of degree ν. Moreover, the scaling parameters are invariant under the addition of a function with an extremum of higher order at the same location. In particular, a *bump function,* that is

a C^∞ function with all derivatives vanishing at the maximum, can be added to the f_ν-family in order to stabilize the $\nu \to \infty$ asymptotics. (Such a function cannot be analytic, but it may be C^∞ on the real line). For example, one could use $\exp(-1/x^2)$. The corresponding sequence of maps

$$g_\nu = 1 - k\left(|x|^\nu + \exp\left(-\frac{1}{x^2}\right)\right) \tag{9}$$

does not share the pathological asymptotics of the f_ν-family. Accordingly, the limits can be inverted and the quantity $\lim_{n\to\infty}\lim_{\nu\to\infty} \delta_n(\nu)$ can be obtained. We will show that this quantity exists, and will calculate it; furthermore, it will be found to coincide within numerical error with the value previously obtained [10] for the reversed limit. Thus, we suggest that this limit is far better behaved than it was previously assumed.

Following the introduction of the g_ν-family, it is natural to use the *inverse Gaussian map*

$$x_{n+1} = \begin{cases} \lambda\left(1 - \exp\left\{-\left(\dfrac{\mu}{x_n - 1/2}\right)^2\right\}\right) & \text{if } x \neq 1/2 \\ \lambda & \text{if } x = 1/2 \end{cases} \tag{10}$$

in order to numerically evaluate $\delta(\infty)$. As already mentioned before, this map has all its derivatives equal to zero at the maximum; furthermore, it is continuous and all derivatives are continuous on the real line. Therefore, this map can be regarded as unimodal with $\nu = \infty$ in the neighborhood of its maximum.

To illustrate the origin of the difficulties that one faces in the numerical study of the above mentioned limits, let us consider the function $F(\lambda) = f_\lambda^{2^n}(x_{\max}) - x_{\max}$, whose zeroes define the λ_n (see Eq. (3)). A short analysis shows that the derivatives of F at its zeroes behave asymptotically as $(-\delta/\alpha)^n$. For the $\nu \to 1^+$ case, this implies that $F(\lambda)$ becomes very flat for relatively small n, and therefore it is numerically

infeasible to determine the location of its zeroes. On the other hand, for the $\nu \to \infty$ case, the derivative increases without bound, and standard numerical methods do not have enough stability to locate the zeroes, whenever these accumulate geometrically with a rate larger than ≈ 25. The typical form of the derivative of F with respect to λ for these two cases is shown in Fig. 2.

These considerations lead us to the necessity of finding a new numerical technique to calculate the $\delta(\nu)$ function. We shall introduce such a technique in the following section.

3. The numerical method

Before discussing the algorithm used in this work to calculate δ, let us review some results from the symbolic dynamics theory on which the method relies.

It is well known that the stable periodic orbits of unimodal maps of the type given by Eq. (1) appear in a universal order (known as MSS after Metrópolis, Stein and Stein)[3] as the parameter λ is increased. The basic tool employed in the proof of this result is the symbolic description of the trajectories. This description consists of associating to each orbit of period n a sequence of n symbols R, L or C, according to the position relative to the critical point of each orbit element, i.e.: R if the corresponding point of the orbit is to the right of the maximum where the derivative of the map with respect to x is negative, L if it is to the left and accordingly the derivative is positive and C if the iterate is at the maximum. It can be shown that the sequence corresponding to a given periodic orbit is the same as the symbolic sequence of a transient, which starts from $x_0 = x_{\max}$; that is, the transient has the same topology as the orbit. Thus, by convention, the orbits always start with $x_0 = x_{\max}$, so as to avoid cyclic permutations of the sequences. It follows that no orbit can have a symbolic description with a C in the middle, since that would imply that the orbit is superstable with a shorter period. Therefore, superstable orbits always end with C. The symbolic description

defined in this way distinguishes between orbits corresponding to values of $\lambda < \lambda_s$ from orbits with $\lambda > \lambda_s$ where λ_s is the superstable point in the region.

Due to several topological constraints, arbitrary sequences of symbols do not necessarily correspond to allowed stable orbits. For example, no sequences may begin with *LR* , because the iterate of the maximum must be greater than the iterate of any other point. It is therefore impossible that the first iterate be in the L zone while the second iterate is in the R zone.

The MSS work leads to an algorithm for the construction of the allowed sequences corresponding to superstable orbits and at the same time specifies the order in which these orbits appear in parameter space. A less publicized result[13] is that the MSS order definition, which is somewhat complicated when defined in terms of the symbolic sequences, can be translated into a quite simple binary tree structure provided that the proper labeling is introduced. In this construction, each node of the tree is associated with a symbolic sequence such that both allowed and forbidden sequences are present. However, the natural order of the nodes which correspond to allowed sequences is precisely the MSS order. In other words, the tree translates the MSS order into the order of real numbers.

The symbolic labeling of the tree proceeds as follows. With each link between two nodes either an *R* or an *L* is associated. The assignment of *R* 's and *L* 's to the links is done horizontally following the order *LRRLLRRL*... (see Fig. 3). Thus, each node represents a symbolic sequence which is obtained by reading the symbols on the corresponding chain of links from the top to the node. Note that the *L* symbol in this labeling indicates *continue in the same direction* while the *R* symbol means *reverse direction.* The relationship between the *L* or *R* symbols and the *absolute* left or right movements on the tree links (labeled in Fig. 3 as *l* or *r*) is known as the *Gray encoding*[14] of the binary sequence, and has been widely used in error correction codes. In order to distinguish between the two labeling schemes we shall refer to the *L* , *R*

symbols as Gray-like and to the l, r symbols as ordinary binary.

There is a simple interpretation to the labeling schemes in terms of a variation, ϵ_n, of the orbit, x_n

$$x_{n+1} + \epsilon_{n+1} = f(x_n) + \frac{df}{dx}(x_n)\,\epsilon_n \tag{11}$$

Namely, the symbolic assignment then proceeds according to the following rule

$$S_n = \begin{cases} R & \text{if } s_n = -1 \\ L & \text{if } s_n = +1 \end{cases}$$

$$s_n = \text{sign}\left(\left.\frac{df}{dx}\right|_{x_n} \right) \tag{12}$$

On the other hand, the sign of the variation, ϵ_n, is

$$v_n = \text{sign}\left(\epsilon_n\right) \equiv \prod_{i=1}^{n} \text{sign}\left(\left.\frac{df}{dx}\right|_{x_n} \right) \tag{13}$$

and consequently, the l, r symbols are defined in terms of v_n

$$V_n = \begin{cases} r & \text{if } v_n = -1 \\ l & \text{if } v_n = +1 \end{cases} \tag{14}$$

In other words, the absolute movements on the tree can be deduced from the sign of the variation at the n-th iterate. We will now see how this is related to the MSS order.

As already mentioned before, this binary tree contains any arbitrary sequence and only a subset of the nodes represent structurally permissible MSS sequences. However, it has been proved[13] that the natural order of the nodes restricted to allowed sequences coincides with the MSS order. We will not reproduce here the details of the proof. Instead, we show in Fig. 4 the coordinate of the nodes which are associated with the symbolic sequences generated by the logistic map ($\nu = 2$), as a function of λ.[15] It is obvious that only the allowed symbolic sequences are produced by the map and, of course, they appear in the MSS order as λ increases. Our statement that the order of

the nodes is the same as the universal MSS ordering, is then reflected by the fact that the graph in Fig. 4 is monotonic.

A second ingredient necessary for our numerical method is also a result from the theory of symbolic dynamics. The symbolic sequence corresponding to the trajectory at the onset of chaos has the following renormalization property: the (infinite) sequence is invariant under the substitution $R \rightarrow RL$ and $L \rightarrow RR$.[16] This may be used to prove that the sequence has a binary tree structure, and, moreover, that this is the same as the last digit 1 in the binary expansion of the natural numbers (see Table I). Accordingly, a straightforward formula for the computation of each symbol S_i in the sequence can be found

$$n_i = \max_k \left\{ k \mid 2^k \text{ divides } i \right\} \tag{15}$$

$$S_i = \begin{cases} R & \text{if } n_i \text{ is odd} \\ L & \text{if } n_i \text{ is even} \end{cases}$$

Furnished with these results, we can easily devise an extremely robust numerical method to detect superstable orbits. Since we are able to recognize whether an orbit produces a symbolic sequence which is before or after the desired superstable one, a bracketing search is possible. This approach assures convergence even for the singular limits mentioned above. More specifically, we iterate the maximum and compare the resulting symbolic sequence with the sought one as defined by Eq. (15). At the step where the two sequences differ, we stop the iteration, reset the λ values and start again from the maximum.

The idea of using symbolic dynamics based algorithms to detect superstable orbits is not completely new. Hao Bai Lin,[17] for instance described a method in which the symbol sequences are used to determine the correct branches of the inverse map in the backward iteration of the critical point. However, this method requires computing the inverse map, a task which in general is more time consuming than computing the map itself.

Therefore, our algorithm presents the additional advantage of requiring only forward iterations.

4. Results

Using the tools developed in the preceding sections, we have computed the index δ as a function of ν for maps of the form

$$x_{n+1} = \lambda \left(1 - |1 - 2x_n|^{\nu}\right) \tag{16}$$

for ν between 1.0015 and 90.

The function $\delta(\nu)$ has been plotted in Fig. 5. It is clearly seen that $\delta(\nu)$ is a smooth monotonically increasing function in agreement with the renormalization group theory.[2,4]

In the following, we analyze our results for the two limits mentioned in Sec. 2, *i.e.* $\nu \to 1$ and $\nu \to \infty$.

a) The $\nu \to 1^+$ limit. While here a well established theoretical result is available ($\delta(\nu \to 1^+) \to 2$), the convergence to the limit is extremely slow. Notice for instance that for $\nu = 1.0015$ we obtained $\delta = 2.2442...$ a value which still differs by more than 10% from the limit. Thus, the question of how $\delta(\nu)$ behaves in this regime naturally arises. Interestingly enough, the attempt to fit a power law to $\delta(\nu - 1) - 2$ around $\nu = 1$ fails in less than one decade. Moreover, the estimates for the exponent yielded by such fits systematically decrease when the data are restricted to intervals closer to $\nu = 1$. This behavior strongly suggests the asymptotic relation

$$(\nu - 1) \approx \exp\{a\,(\delta - 2)^{-b}\} \tag{17}$$

or

$$\log(\nu - 1) \approx \frac{a}{(\delta - 2)^b} + c \tag{18}$$

for small values of $(\nu - 1)$. Although the multiplicative constant before the exponential

is uncertain, one would expect a reasonable estimate for the exponent b and the constant a from the data close to ν=1. In Fig. 6 we have plotted $\log(-\log(\nu-1)-c)$ versus $\log(\delta-2)$ for several values of c. The graph becomes linear for small values of $\delta-2$. This confirms our hypothesis concerning the asymptotic behavior and allows us to estimate the value of the index b as the slope of the linear part. Moreover, the quality of the linear fit is best for $c \approx 1.25$ and this leads to $b \approx .46$. We will return to these results later when we discuss the global shape of $\delta(\nu)$.

b) The $\nu \to \infty$ limit. At first glance, the shape of the $\delta(\nu)$ curve shown in Fig. 7 could support equally well both the hypothesis of a $\sqrt{\nu}$ divergence or the existence of a finite asymptotic limit. However, as we shall see, a more refined analysis shows a tendency which is compatible with the existence of the above mentioned upper bound. To further clarify this issue one could proceed with the computation of δ for increasingly higher (but finite) values of ν. However, this approach becomes impractical above $\nu \approx 100$. Instead, we study the bifurcation sequence for the map in Eq. (10) which can be regarded as belonging to the $\nu = \infty$ universality class. In Table II the values of the bifurcation ratios $\delta_n(\infty)$ are listed (corresponding to the n-th and $(n-1)$-th bifurcations) for n between 4 and 18. A slow but monotonic convergence to $\delta(\infty) \approx 30$ can be observed. Moreover, an improvement to the estimation for $\delta(\infty)$ can be achieved by means of the following method. Let us first define the function $\delta(q) \equiv \delta_n(\infty)$ where $q = 1/n$ such that

$$\delta(\infty) = \lim_{q \to 0} \delta(q) \tag{19}$$

We know that $\delta(q)$ is monotonic, since it converges geometrically for the even and odd subsequencies, with a positive factor; for the same reason, the even and odd subsequencies are convex, and are intertwined. We then use these facts in the neighborhood of $q = 0$ to assure that the value of the limit is bounded between $\delta(q)$ and its Legendre transform

$$\gamma(q) = \delta(q) - q\frac{d\,\delta}{dq} \tag{20}$$

Moreover, it can be shown, that

$$\bar{\delta}(q) = \frac{\delta(q)+\gamma(q)}{2} = \delta(\infty) + O(q^3) \tag{21}$$

indicating that the average $\bar{\delta}(q)$ should display accelerated convergence to the limit (see Fig. 7). This procedure leads to the result $\delta(\infty) = 29.8...$ which is in agreement with the analytic estimate made in Ref. 9 by means of renormalization group arguments.

c) The global form of $\delta(\nu)$. An interesting feature in the global dependence of the bifurcation rate δ on the order of the maximum is revealed in Fig. 8. In Fig. 8(a) we show the numerical derivative δ_s' of the function $\delta_s(\nu_s)$ where $\delta_s = \delta - 2$ and $\nu_s = \log(\nu - 1)$. Notice that δ_s' has a maximum at $\nu_s \approx 1.25$ which coincides with the value of c mentioned above as the one optimizing the fit to the law of Eq. (18). Since our data are poorer as the order ν increases, the curve δ_s' becomes noisy after this maximum. However, there is substantial evidence supporting the conjecture that δ_s' is symmetric around its maximum. On the basis of this hypothesis, we can predict the value of $\delta(\infty)$ using the results from the small ν part of $\delta(\nu)$. This estimation leads to $\delta(\infty) \approx 31.2$ which coincides with the actual value within 5%. Accordingly, Fig. 8(b) illustrates the conjectured symmetry of the function $\delta_s(\nu_s)$.

A true confirmation of this symmetry should come from the systematic computation of $\delta(\nu)$ for increasing values of $\log(\nu - 1)$. Results of the work in progress on this problem will be discussed elsewhere.

5. Conclusions

We have introduced a symbolic dynamics based procedure to economically perform large scale calculations of the scaling indexes for period doubling bifurcation sequences. With the help of such an algorithm we have calculated with great precision the function

$\delta(\nu)$ over a broad range of ν values. In the $\nu \to 1^+$ limit we could conclude that the theoretical $\delta = 2$ result can only be reached for values of ν exponentially close to 1. On the other hand, we have confirmed the existence of a finite limit for $\delta(\nu \to \infty)$ giving, at the same time, an accurate estimate for its value. Finally, we presented evidence supporting the conjecture that the behavior of the index δ for exponentially large values of the parameter ν is symmetric to its behavior for ν exponentially close to 1. If confirmed, the predictive ability of this conjecture would be extremely helpful in completing the analysis of the universal metric properties dependence on the order of the critical point.

Acknowledgments

We would like to thank E. Fradkin, H. Fanchiotti, M. Santangelo and H. Vucetich for many helpful discussions, suggestions and criticisms. M.O.M. thanks P. Glendining for some helpful remarks. This work has been supported in part by NSF-DMR under grant number 85-19460, by Consejo Nacional de Investigaciones Científicas y Técnicas of the Republic of Argentina and by the Director, Office of Energy Research, Office of High Energy and Nuclear Physics, Division of Nuclear Physics of the U.S. Department of Energy under Contract No. DE-AC03-76SF00098. One of us (M.F.) acknowledges financial support from the Dr. Chaim Weizmann foundation. Part of this work was done while O.P. was visiting the Center for Nonlinear Studies at the Los Alamos National Laboratory. He thanks D.J. Farmer for his warm hospitality.

References

1. M. J. Feigenbaum, *J. Stat. Phys.*, **19**, 25 (1978).
2. M. J. Feigenbaum, *J. Stat. Phys.*, **21**, 669 (1979).
3. N. Metropolis, J. L. Stein, and P. R. Stein, *J. Combinatorial Theory*, **15**, 25 (1973).
4. P. Collet and J. P. Eckmann, *Iterated maps on the interval as dynamical systems*, (Birkhauser, Basel, 1980).
5. Some additional conditions are required but we can safely consider maps of the form $f\ (\mid x \mid^{\nu})$ where f is a smooth monotonic function.
6. B. Hu, *Phys. Rep.*, **91**, 233 (1982).
7. P. R. Hauser, C. Tsallis, and E. Curado, *Phys. Rev. A*, **30**, 2074 (1984).
8. J. P. Eckmann and P. Wittwer, *Computer methods and Borel summability applied to Feigenbaum's equation*, Lecture Notes in Physics, 227, (Springer, Berlin, 1985).
9. J. P. van der Weele, H. W. Capel, and R. Kluiving, *Phys. Lett. A*, **119**, 15 (1986).
10. J.P. van der Weele, H.W. Capel, and R. Kluiving, *Physica A*, **145**, 425 (1987).
11. B. Derrida, A. Gervoise, and Y. Pomeau, *Ann. Inst. Henri Poincare*, **29**, 305 (1978).
12. See for instance B. Hu and J. M. Mao, *Phys. Rev. A*, **25**, 3259 (1982).
13. D. L. Gonzalez, PhD Thesis, Universidad Nacional de La Plata, La Plata, 1987.
14. R.W. Hamming, *Coding and Information Theory*, (Prentice-Hall, New Jersey, 1986).
15. The coordinate of a node is given by its binary address. However, any other uniform assignment of coordinates (for example the rational number associated with each node of a Farey tree) is equally suitable for the purpose of the demonstration, provided that the branches do not cross each other.
16. This follows from S = R * S, where S is the onset of chaos sequence, and * is the sequence product defined by MSS

17. B. L. Hao, "Symbolic Dynamics," ICTP Lectures Notes, ICTP, Trieste, 1986.

Decimal i	Binary i	n_i	MSS S_i	Tree structure
1	0001	1	R	
2	0010	2	L	
3	0011	1	R	
4	0100	3	R	
5	0101	1	R	
6	0110	2	L	
7	0111	1	R	
8	1000	4	L	
9	1001	1	R	
10	1010	2	L	
11	1011	1	R	
12	1100	3	R	
13	1101	1	R	
14	1110	2	L	
15	1111	1	R	

Table I. The binary expansion of the first fifteen natural numbers and its relation to the corresponding members of the symbolic sequence for the 2^{∞} orbit at the onset of chaos. n_i is given either by Eq. (15) or equivalently by counting the position of the (underlined) last digit 1 from left to right. Eq. (15) also gives the translation from n_i to the i-th symbol of the period doubling attractor. The underlaying tree structure is generated recursively starting from the lowest levels.

n	$\tilde{\delta}(1/n)$	$\tilde{\gamma}(1/n)$	$\bar{\delta}(1/n)$
4	15.84423	33.18954	24.51688
5	19.80478	35.79244	27.79861
6	22.49363	36.32217	29.40790
7	24.52404	35.93053	30.22728
8	25.85286	34.96990	30.41138
9	26.84534	34.07744	30.46139
10	27.49777	33.18256	30.34016
11	27.99756	32.50903	30.25330
12	28.33298	31.91092	30.12195
13	28.59962	31.48098	30.04030
14	28.78270	31.10806	29.94538
15	28.93408	30.84240	29.88824
16	29.04016	30.61049	29.82532
17	29.13130	30.44494	29.78812
18	29.19625		

Table II. The convergence to δ_∞ of $\tilde{\delta}$, $\bar{\gamma}$ and $\bar{\delta}$ for the inverse Gaussian map (see text and Fig. 7).

Figure Captions

Figure 1.

The trajectory scaling exponent, α vs. ν as obtained from Eq. (7).

Figure 2.

The numerical difficulty in locating the superstable cycles in the $\nu \to 1^+$ and $\nu \to \infty$ limits is a consequence of the pathological form the function $F_\lambda = f_\lambda^{2^n}(x_{\max}) - x_{\max}$ assumes in the neighborhood of its zeroes, λ_n. Here, the value of n was set to 10. In the $\nu \to 1^+$ limit (a) the derivative of $F_\lambda(x_{\max})$ with respect to λ around λ_n becomes vanishingly small while in the $\nu \to \infty$ limit (b) it diverges for large n. The arrows indicate the locations of the zeroes of $F(\lambda)$.

Figure 3.

The binary tree with both the Gray and the binary labeling. The former orders the periodic orbits in parameter space. The symbolic sequence of a periodic orbit of length n corresponds to a path on the tree which is of length n and starts at its top. At the n-th level of the tree, scanning the nodes from left to right one encounters periodic orbits in the MSS order.

Figure 4.

The binary assigned node coordinates for the binary tree in Fig. 3 vs. the value of λ at which the corresponding periodic orbits are superstable for the logistic map ($\nu = 2$).

Figure 5.

δ vs. ν for the range $\nu \in (1.0015, 90)$.

Figure 6.

The $\nu \to 1^+$ limit: the behavior of $\log(\log(\nu - 1))$ as a function of $\log(\delta - 2)$ is shown to be linear for small values of $(\delta - 2)$ (see Eqs. 17 and 18). The exact value of c

does not affect this trend.

Figure 7.

The $\nu \to \infty$ limit: the convergence of $\tilde{\delta}(q)$ (dotted line), $\tilde{\gamma}(q)$ (dashed), and $\overline{\delta}(q)$ (continuous) for the inverse Gaussian map (see Eqs. 10, 19, 20 and 21).

Figure 8.

The global form of $\delta(\nu)$: a) $\delta_s{}'$ vs. ν_s (see text), b) δ_s vs. ν_s where the continuous line represents the same data as in Fig. 5 and the dashed curve is obtained by inverting the low ν data with respect to the point $\nu_s = 1.25$.

Fig. 1

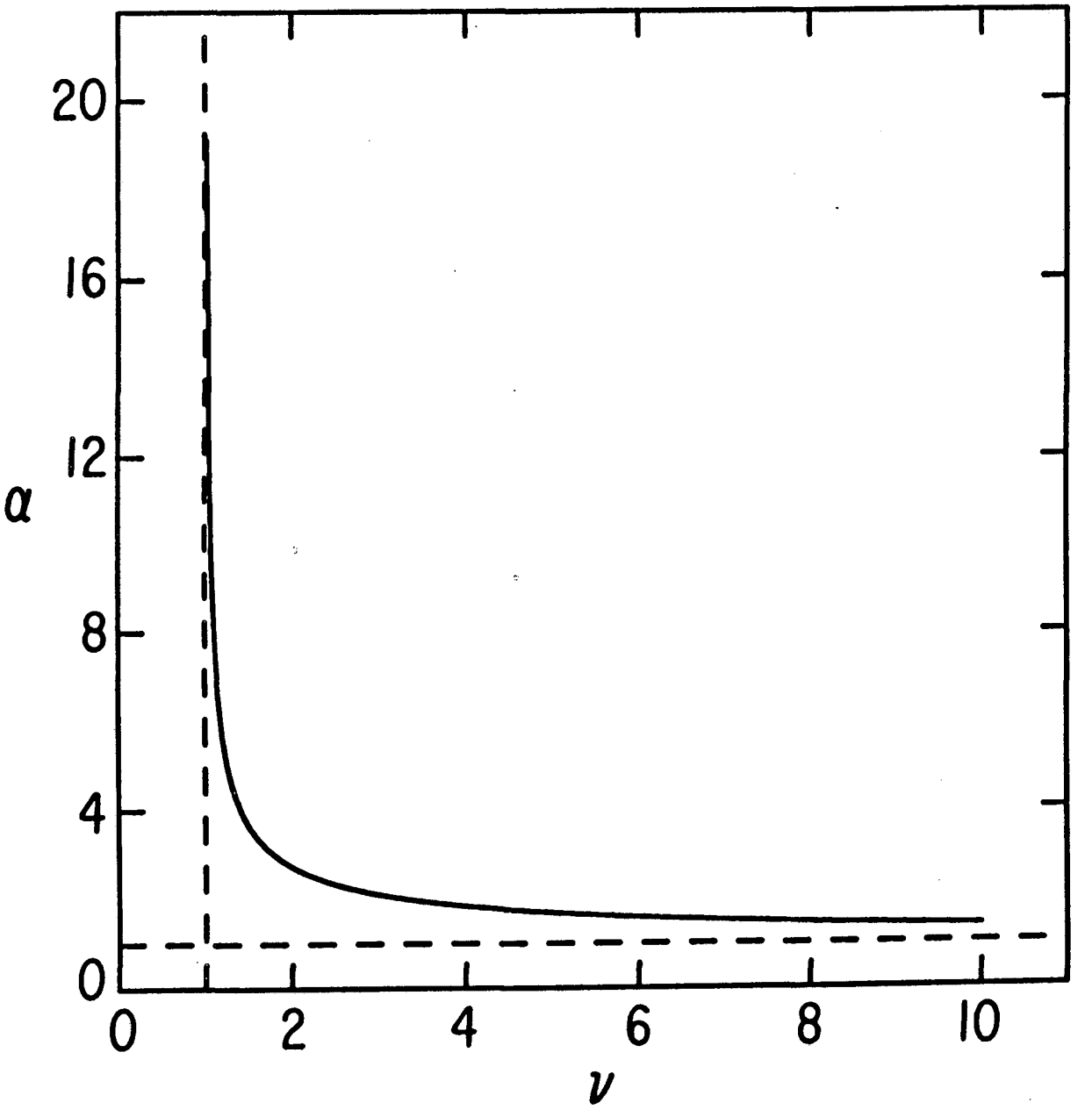

Fig. 2a

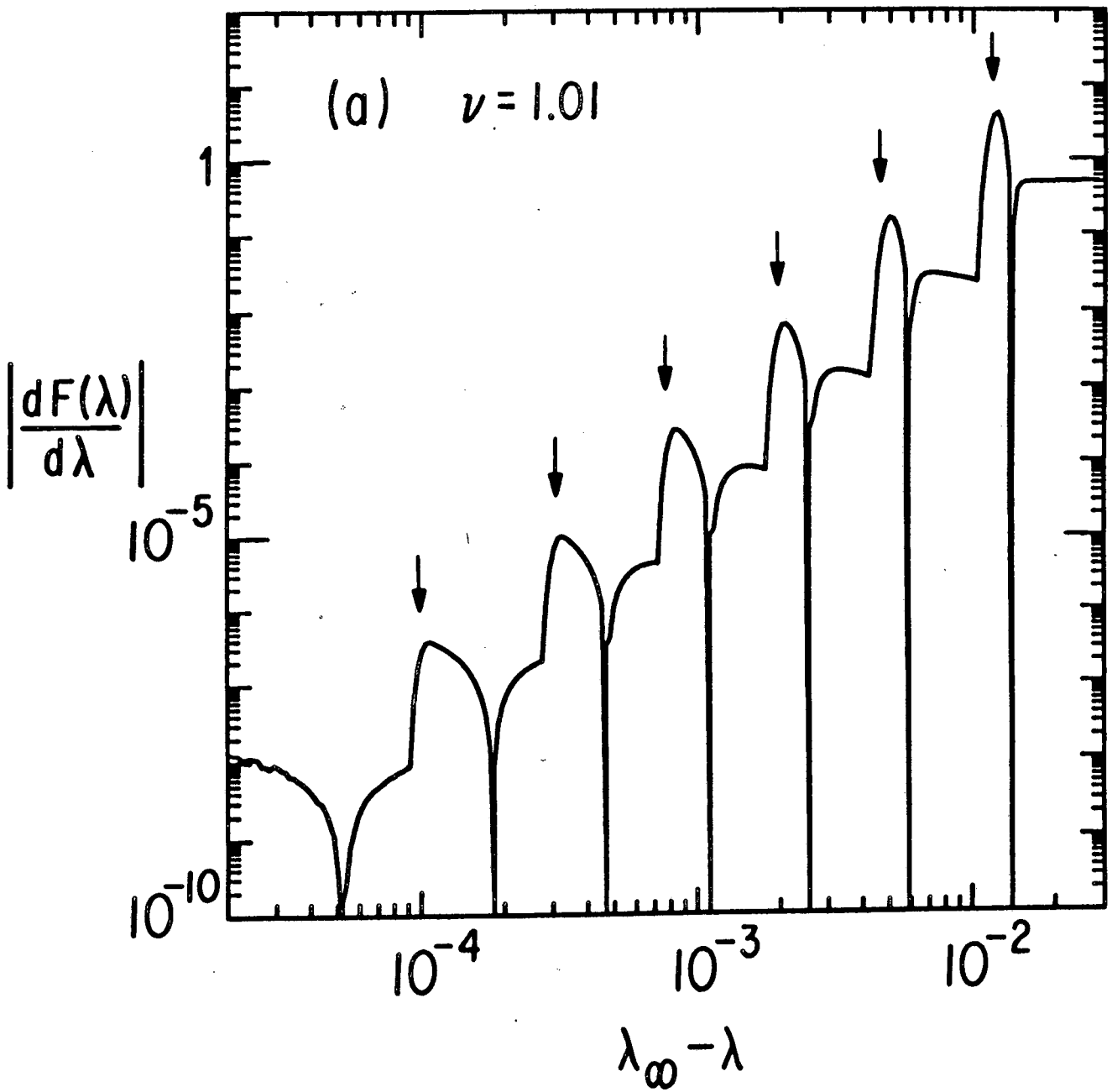
(a) $\nu = 1.01$
1
10^{-5}
10^{-10}
$\left|\frac{dF(\lambda)}{d\lambda}\right|$
10^{-4}
10^{-3}
10^{-2}
$\lambda_\infty - \lambda$

$\left|\frac{\gamma_p}{F(\gamma)}\frac{dF(\gamma)}{d\gamma}\right|$
1
10^3
10^6
$\gamma - \infty\gamma$
10^{-1}
10^{-4}
10^{-7}
$10 = \nu$ (b)

Fig. 2b

Fig. 3

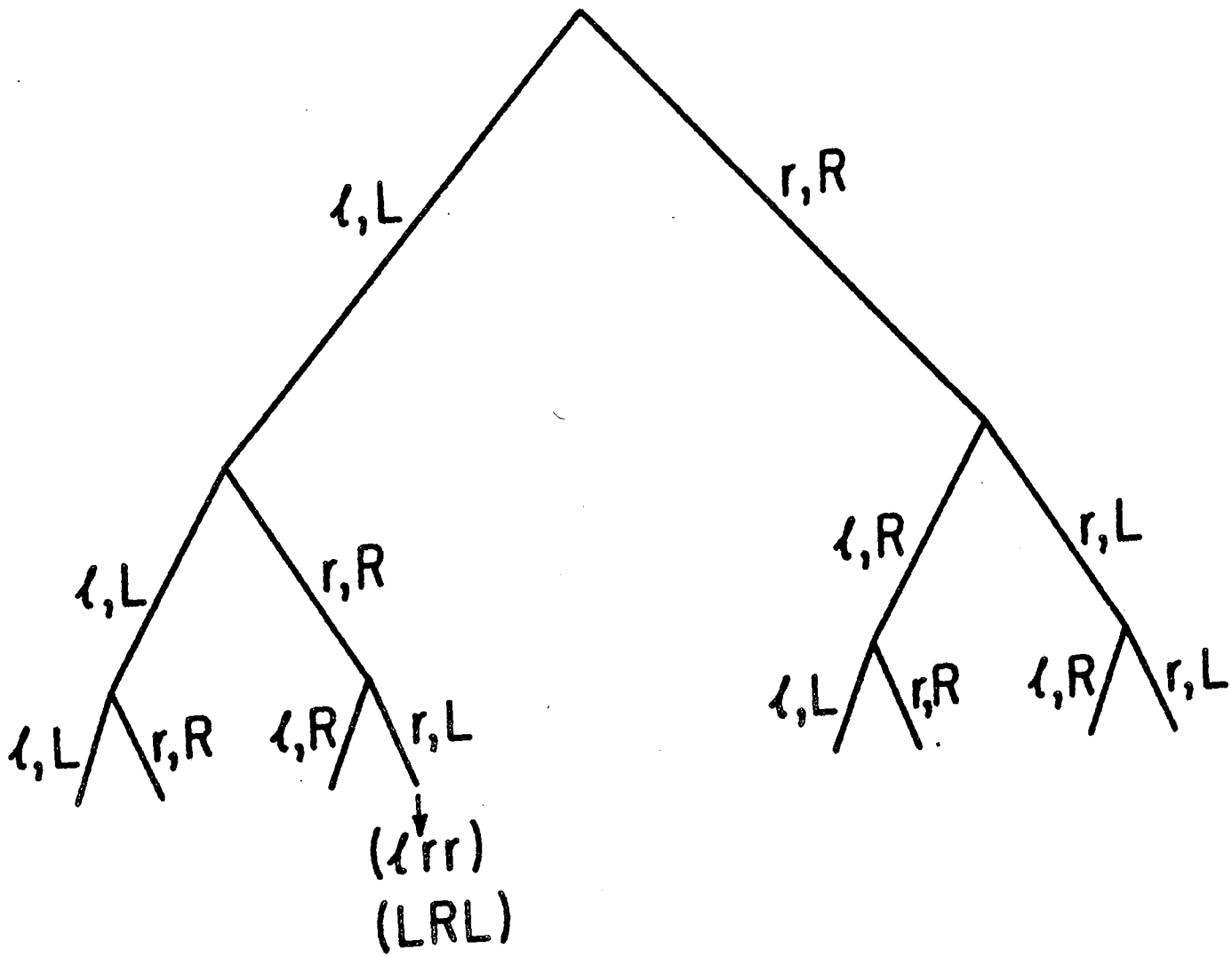

Fig. 4

Fig. 5

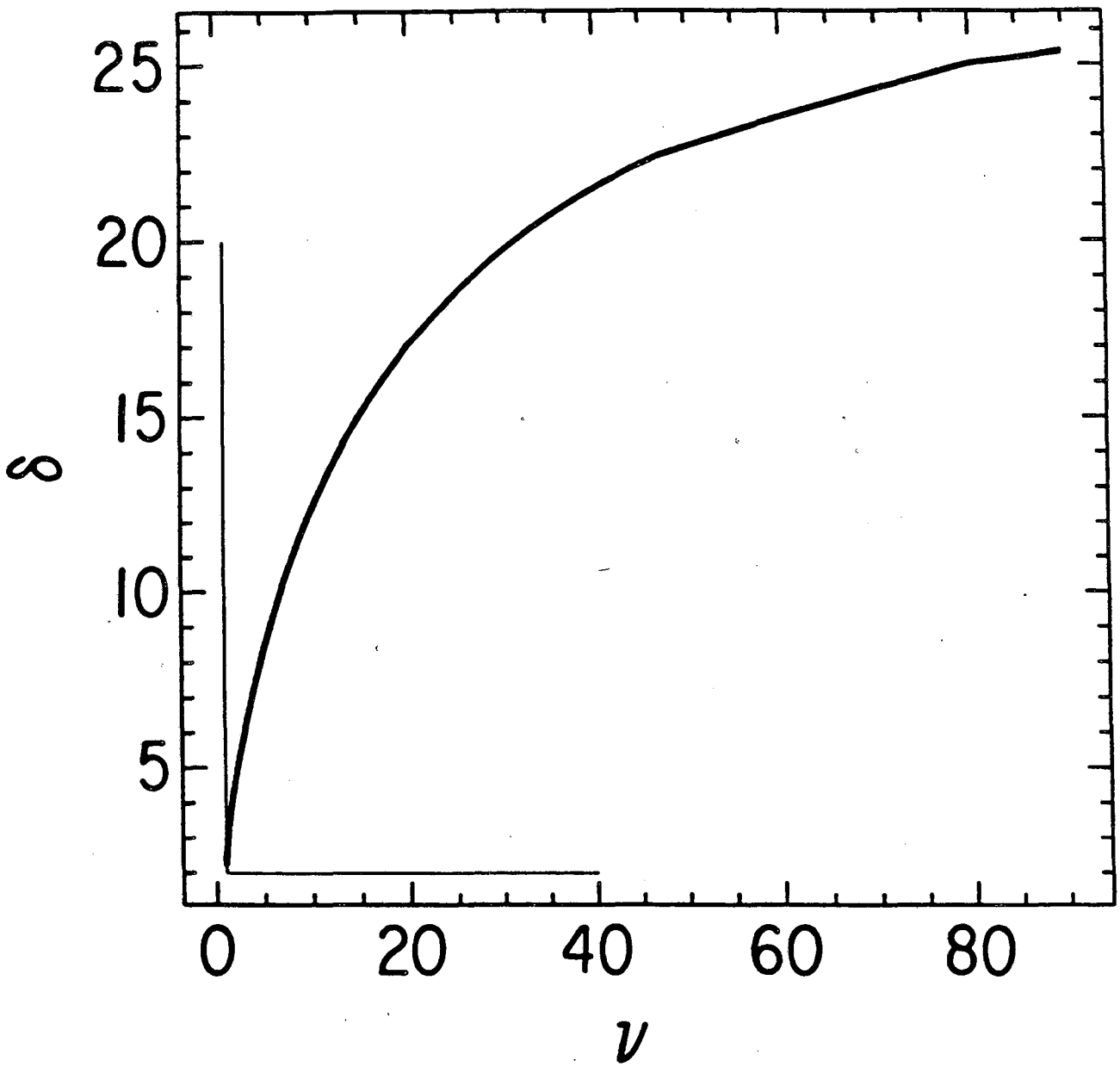

Fig. 6

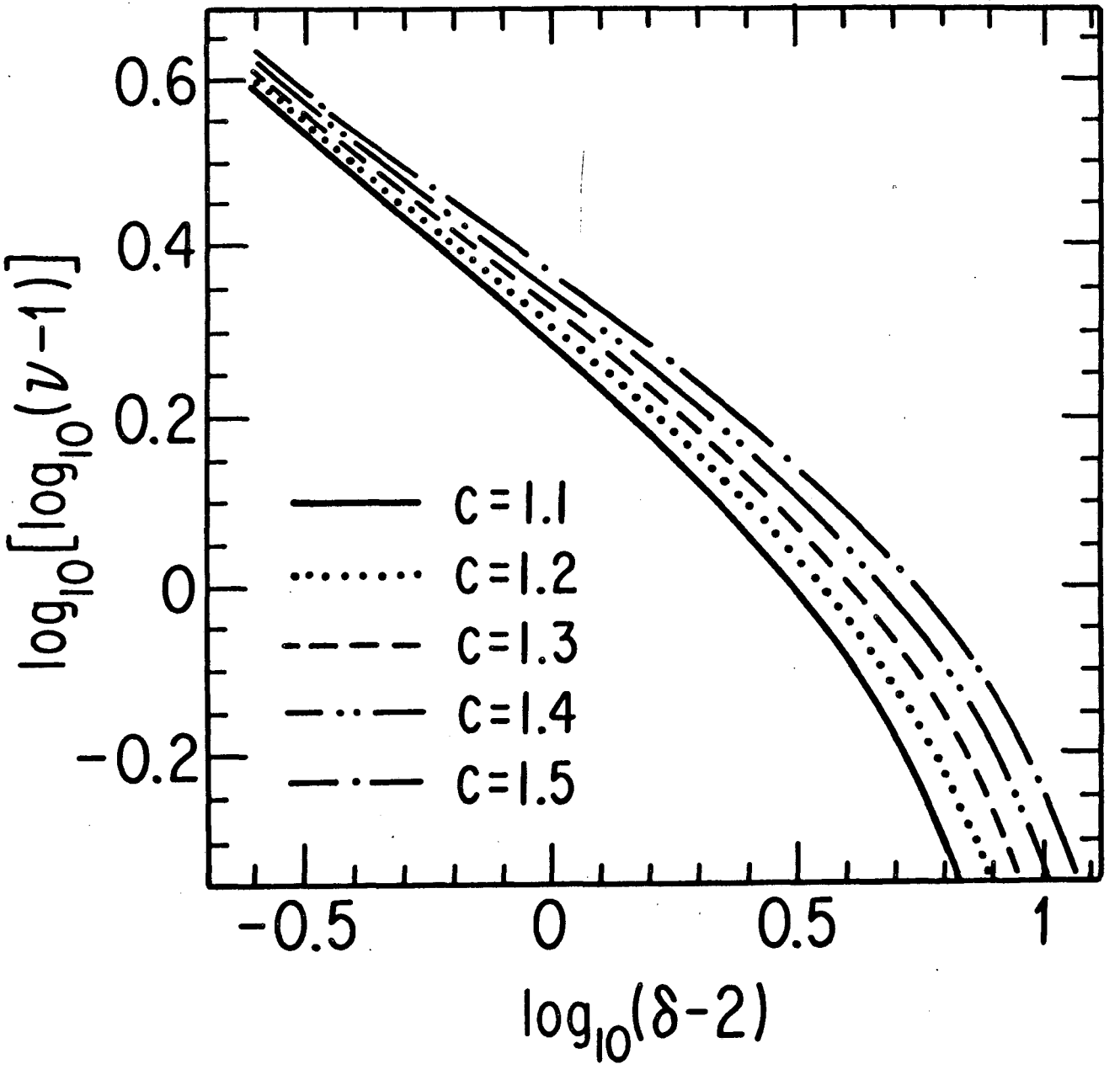
0.6
0.4
0.2
0
−0.2
−0.5
0
0.5
1
$\log_{10}[\log_{10}(\nu-1)]$
$\log_{10}(\delta-2)$
c=1.1
c=1.2
c=1.3
c=1.4
c=1.5

Fig. 7

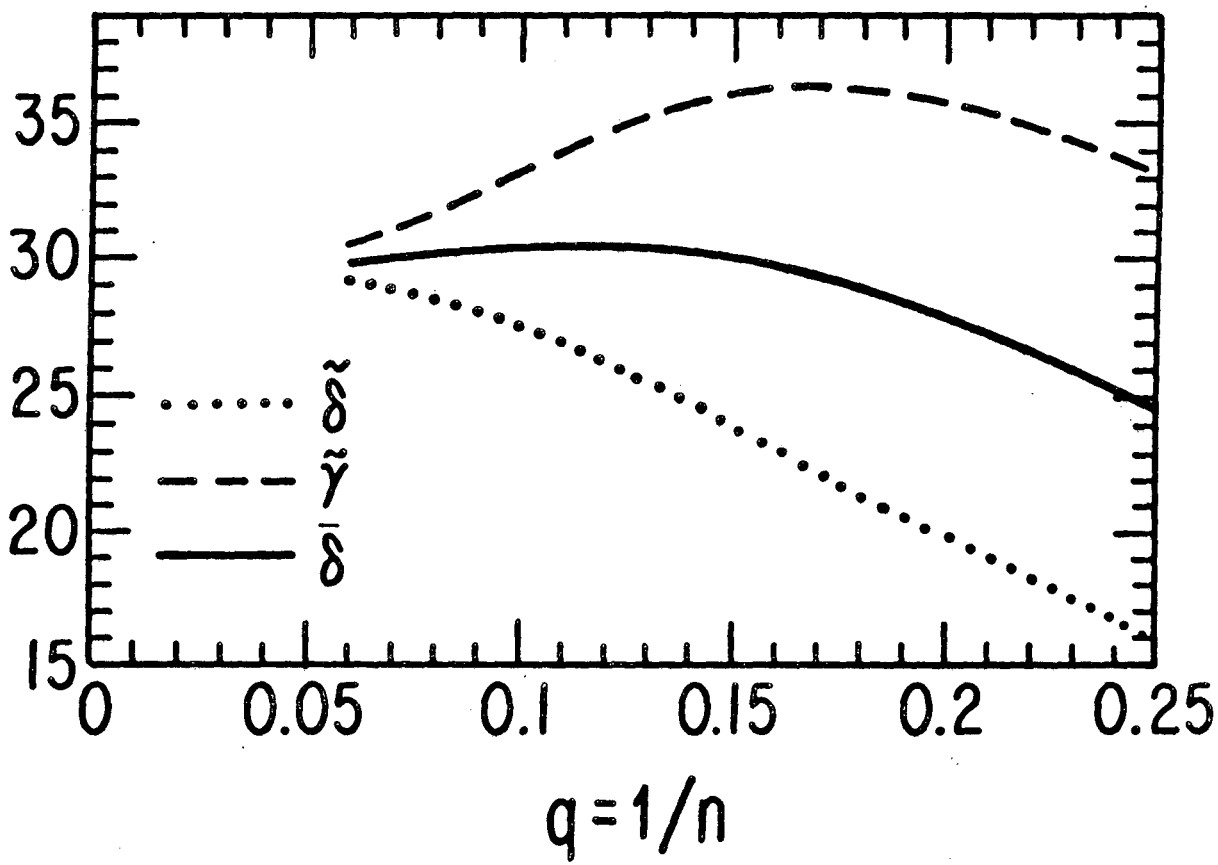
35
30
25
20
15
0
0.05
0.1
0.15
0.2
0.25
$\tilde{\delta}$
$\tilde{\gamma}$
$\bar{\delta}$
q=1/n

Fig. 8a

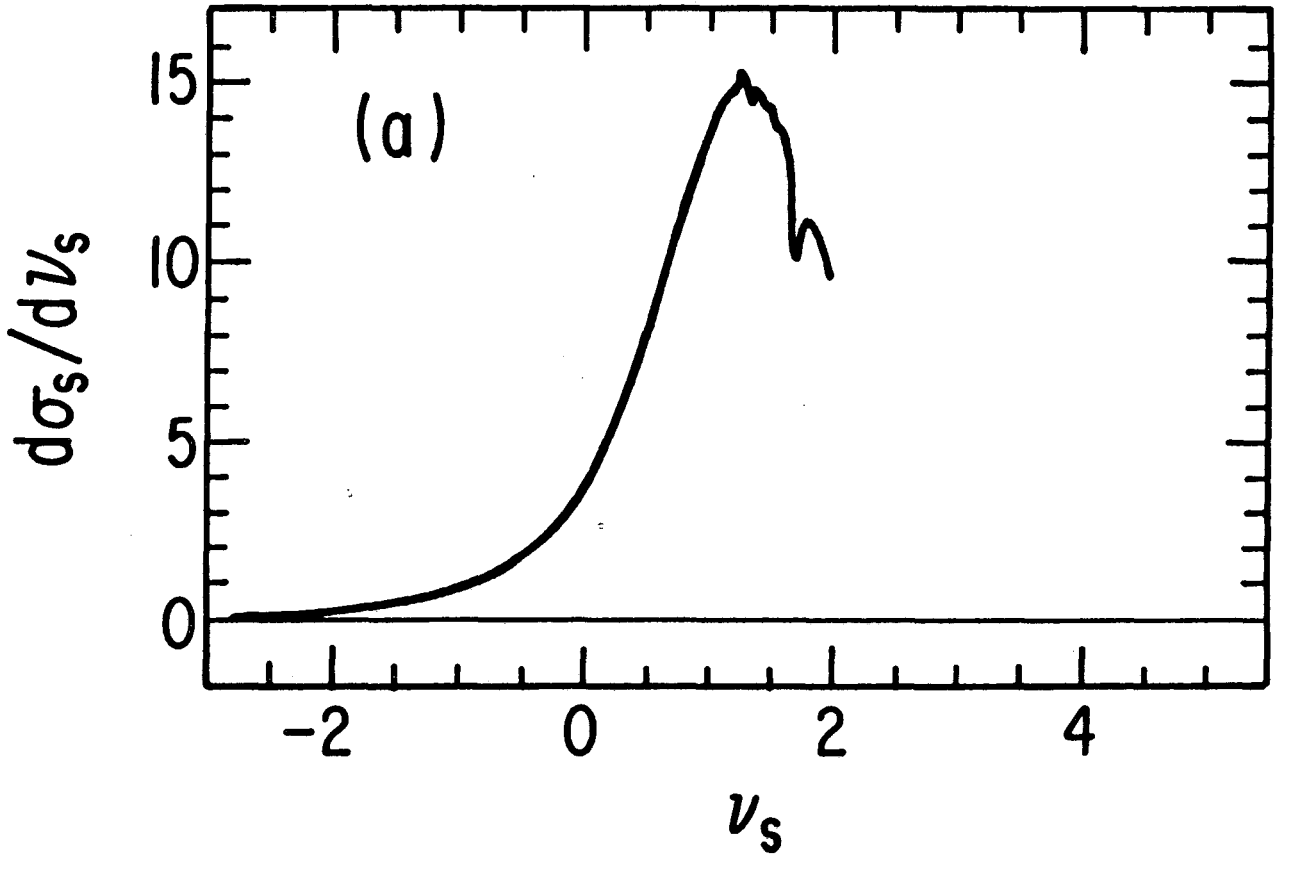

Fig. 8b

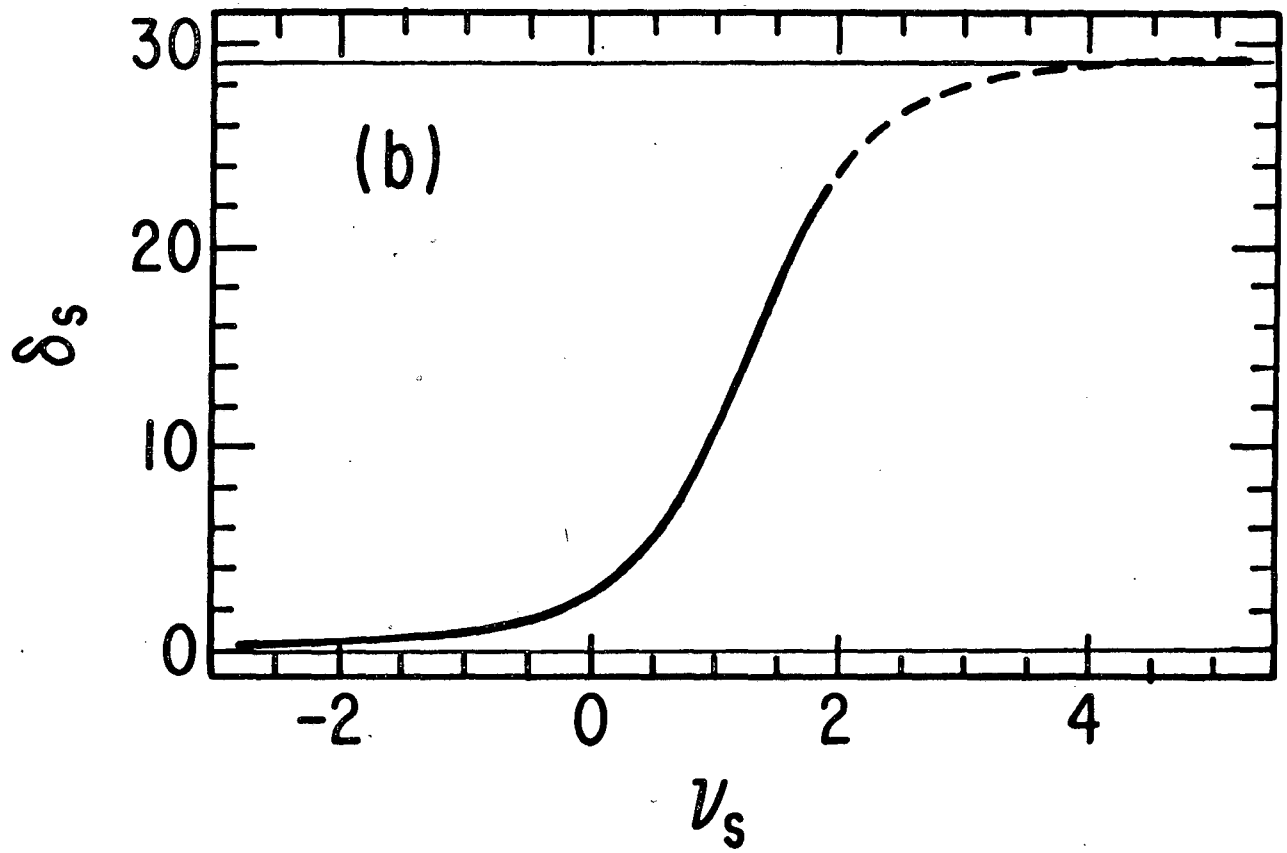

LAWRENCE BERKELEY LABORATORY
TECHNICAL INFORMATION DEPARTMENT
1 CYCLOTRON ROAD
BERKELEY, CALIFORNIA 94720